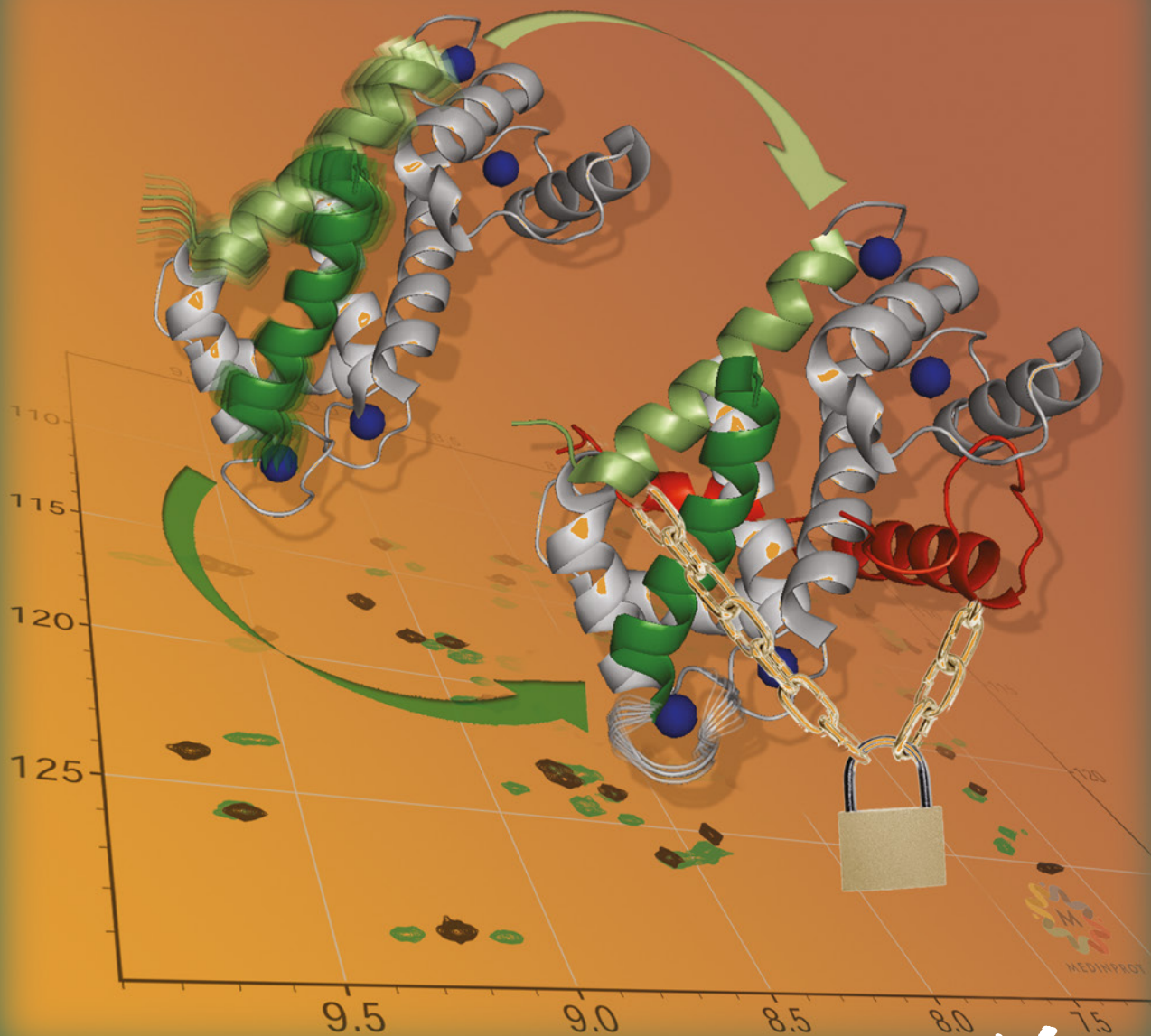


A EUROPEAN JOURNAL OF CHEMICAL BIOLOGY

CHEMBIOCHEM

SYNTHETIC BIOLOGY & BIO-NANOTECHNOLOGY



19/2016

Chemistry & Life Sciences

Front Cover:

L. Nyitray, A. Bodor et al.

Multilevel Changes in Protein Dynamics upon Complex Formation
of the Calcium-Loaded S100A4 with a Nonmuscle
Myosin IIA Tail Fragment

A Journal of



WILEY-VCH

www.chembiochem.org



Multilevel Changes in Protein Dynamics upon Complex Formation of the Calcium-Loaded S100A4 with a Nonmuscle Myosin IIA Tail Fragment

Gyula Pálffy,^[a] Bence Kiss,^[b] László Nyitrai,^{*,[b]} and Andrea Bodor^{*,[a]}

Dysregulation of Ca²⁺-binding S100 proteins plays important role in various diseases. The asymmetric complex of Ca²⁺-bound S100A4 with nonmuscle myosin IIA has high stability and highly increased Ca²⁺ affinity. Here we investigated the possible causes of this allosteric effect by NMR spectroscopy. Chemical shift-based secondary-structure analysis did not show substantial changes for the complex. Backbone dynamics revealed slow-timescale local motions in the H1 helices of homodimeric S100A4; these were less pronounced in the com-

plex form and might be accompanied by an increase in dimer stability. Different mobilities in the Ca²⁺-coordinating EF-hand sites indicate that they communicate by an allosteric mechanism operating through changes in protein dynamics; this must be responsible for the elevated Ca²⁺ affinity. These multilevel changes in protein dynamics as conformational adaptation allow S100A4 fine-tuning of its protein–protein interactions inside the cell during Ca²⁺ signaling.

Introduction

S100 proteins are vertebrate-specific Ca²⁺-binding proteins of low molecular weight (10–12 kDa) with high sequence similarity. They exist mostly as homodimers with subunits held together by non-covalent bonds. Each monomer contains two helix-loop-helix EF-hand-type motifs to bind Ca²⁺.^[1,2]

Our main focus is on S100A4, which is found in the cytoplasm, in the nucleus, and in the extracellular space. It has gained increasing attention over recent decades because of its metastasis-promoting properties, as well as its role in the pathogenesis of rheumatoid arthritis and in fibrotic diseases.^[3] It has been shown that the expression level of S100A4 correlates with the invasiveness of several cancer cell lines; a direct role of S100A4 in tumor metastasis was demonstrated in animal models. Clinical studies have revealed that S100A4 expression is a significant prognostic marker of aggressive tumors associated with poor survival rate.^[3–8] Therefore, atomic level in-depth characterization of the interaction between S100A4 and its target proteins is essential.

The structures of apo and Ca²⁺-bound S100A4 have been determined both by solution NMR spectroscopy and X-ray crystallographic diffraction.^[9–14] All the distinctive structural elements characteristic for S100 proteins are present: the pseudo-

EF hand near the N terminus (formed by helices H1 and H2, which surround loop L1), a connecting “hinge” (L2) and the canonical EF-hand close to the C terminus (L3 loop flanked by helices H3 and H4). The two subunits are held together by an “X-type” four-helix bundle comprising H1 and H4 from each monomer. The apo form shows a closed conformation, but the Ca²⁺-bound form appears to be in an open conformation, with a hydrophobic pocket formed by L2 and parts of H3 and H4. Target proteins bind almost exclusively to the open state. The main binding partners of S100A4 are cytoskeleton proteins (nonmuscle myosin IIA, tropomyosin, F-actin),^[15–17] signal proteins (liprin β 1),^[18] transcription factor p53,^[19] and the non-EF-hand Ca²⁺- and lipid-binding annexin A2.^[20]

Interaction of S100A4 with nonmuscle myosin IIA (NMIIA) is thought to be associated with increased cell migration of metastatic cells.^[1] Previous studies have shown that S100A4 inhibits the assembly of nonmuscle myosin filaments and promotes their disruption.^[21,22] S100A4 colocalizes with NMIIA at the leading edge of migrating cells and regulates directional motility through direct interaction with NMIIA.^[23,24] The S100A4:NMIIA complex has remarkably high affinity ($K_d \approx 0.1$ nM),^[25–27] and its 1:2 stoichiometric structure is unusually asymmetric: a single NMIIA chain bridges the two identical hydrophobic pockets, and hence the equivalence of the two monomers is lost.^[14,25–27] The S100A4-binding region of NMIIA comprises the C terminus of the coiled-coil dimer and part of the nonhelical tailpiece.^[25,26]

Despite several structural studies and investigations of the solution dynamics of the apo and Ca²⁺-bound forms in this protein family (backbone dynamics data are available for apo S100A1,^[28,29] S100A4,^[30] S100A5,^[31] S100A13,^[32] S100A14,^[33] S100B,^[34] and for Ca²⁺-bound S100A1,^[35] S100A5,^[31] S100B^[36] backbone dynamics data are available), only one study has

[a] G. Pálffy, A. Bodor

Laboratory of Structural Chemistry and Biology
Institute of Chemistry, Eötvös Loránd University
Pázmány Péter sétány 1A, 1117 Budapest (Hungary)
E-mail: abodor@chem.elte.hu

[b] B. Kiss, L. Nyitrai

Department of Biochemistry, Eötvös Loránd University
Pázmány Péter sétány 1/C, 1117 Budapest (Hungary)
E-mail: nyitrai@elte.hu

Supporting information for this article can be found under <http://dx.doi.org/10.1002/cbic.201600280>.

investigated the changes in dynamic properties upon target binding (S100B in complex with peptide TRTK).^[37]

In order to understand the regulatory function of S100 family members, the structural and dynamics changes upon Ca^{2+} and protein–ligand binding are highly important. The “S100 dilemma” is that the Ca^{2+} affinity for most S100 proteins is low ($K_d > 10 \mu\text{M}$); therefore they might not be sufficiently saturated to function as switches for Ca^{2+} signaling.^[38] The dilemma might be solved by the fact that Ca^{2+} affinity increases significantly in the presence of target proteins, as demonstrated for S100A1, S100B, and S100A4.^[10,39–42] On the other hand, the low Ca^{2+} affinity could prevent a high concentration of S100 protein from sequestering free Ca^{2+} in the cytoplasm. Tight binding of NMIIA to S100A4 is thermodynamically linked to nanomolar Ca^{2+} affinity in the protein complex. Consequently these two proteins can partially interact even at basal Ca^{2+} levels inside the cell, where the concentration is in the micromolar range.^[26,39,43] The increased Ca^{2+} affinity can be explained by changes in either the structure or dynamics (or both) of the S100A4:NMIIA complex compared to Ca^{2+} -bound S100A4.

In order to obtain greater insight into the intramolecular communications of S100A4 functional sites, we conducted a comprehensive NMR spectroscopic investigation into the structural aspects and solution dynamics of 1) a 45-residue S100A4-binding fragment of NMIIA, and 2) C-terminal-truncated S100A4 in Ca^{2+} -bound form in complex with NMIIA.

Results and Discussion

Resonance assignments and secondary-structure information

MPT is disordered with a transient α -helix in the central region. MPT, the full binding region of NMIIA (residues 1893–1937 of the heavy-chain sequence of NMIIA), forms a high-affinity asymmetric complex with S100A4 dimers.^[25] Of these 45 residues, crosspeaks of the first two could not be detected; all others (excluding P1927 and P1931) appeared in the $^1\text{H},^{15}\text{N}$ HSQC spectrum at low temperatures (Figure 1A). Signal dispersion of the ^1H dimension was 0.6 ppm, in full accordance with a lack of secondary structure. Moreover, several minor peaks ($\sim 10\%$ signal intensity) appeared for residues preceding the prolines. CC(CO)NH spectra revealed that both prolines in the major form are in the *trans* configuration, on the basis of C^β – C^γ chemical shift differences (4.6 ppm for P1927, 4.7 ppm for P1931). SSP values were calculated from the assigned chemical shifts (Figure 1B),^[44] and these confirmed the fully disordered character of MPT. One exception was the central core (D1908–K1918), which presents larger values (>0.3), thus indicating higher propensity for an α -helical structure. In full-length NMIIA this region is part of the coiled-coil tail, but in the S100A4:MPT crystal complex it forms an amphipathic α -helix bridging the S100A4 dimer interface.^[25,26]

Temperature coefficients (ppb/K) were calculated from the temperature dependence of the ^1H chemical shifts derived from HSQC spectra in the 288–310 K range. In the M1910–R1922 region the values were smaller than the average value, thus indicating that this is a more rigid part of the molecule

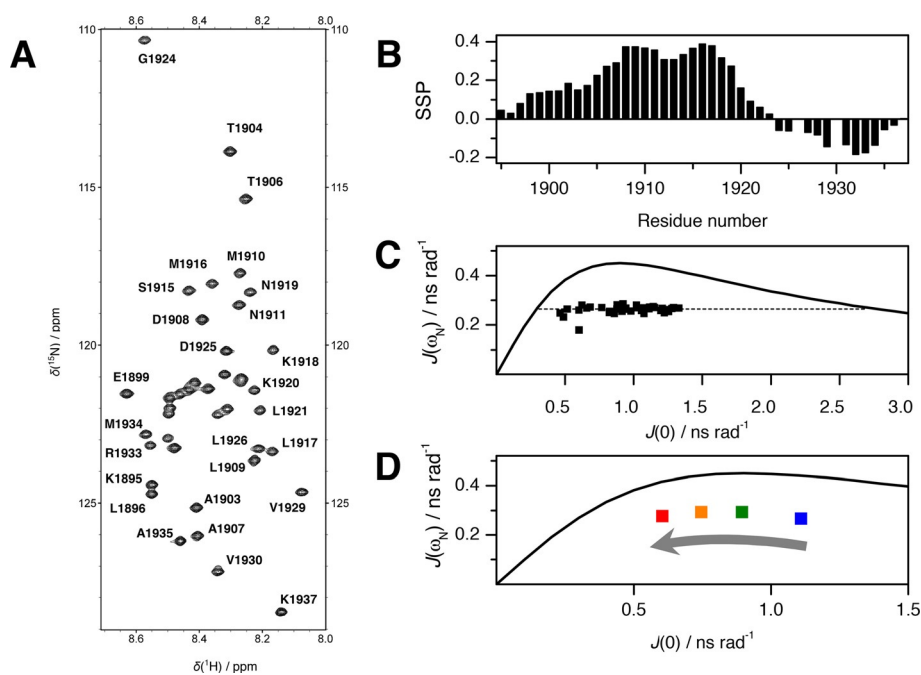


Figure 1. A) Assigned $^1\text{H},^{15}\text{N}$ HSQC spectrum of MPT (residues 1893–1937 of NMIIA) measured at 700 MHz at 283 K. B) Calculated SSP scores along the amino acid sequence. C) Reduced spectral density analysis at 283 K for all backbone residues. D) Reduced spectral density for residue A1907 at 283 K (blue), 288 K (green), 293 K (orange), and 298 K (red).

(the obtained slopes along the amino acid sequence are shown in Figure S1A in the Supporting Information). A comparison with the Eisenberg hydrophobicity index (Figure S1B) revealed that large temperature coefficients are characteristic for regions with a more pronounced hydrophobic character (L1926–V1930). This correlation indicates that a small hydrophobic core might form temporarily in the neighborhood of proline residues; this might contribute to the adoption and initialization of a folded structure upon complex formation.

Comparison of free and MPT-bound S100A4dC structures. A C-terminally 13 residues truncated form of Ca²⁺-bound S100A4 (S100A4dC) was used, in order to avoid the aggregation tendency of full-length S100A4. Previous studies indicated that MPT binding is not affected by this C-terminal truncation.^[14,27,43]

The ¹H,¹⁵N HSQC spectrum of S100A4dC has well-dispersed resonances, as expected for a folded protein. Backbone resonance signals were assigned over M1–E88 (Figure 2), and the

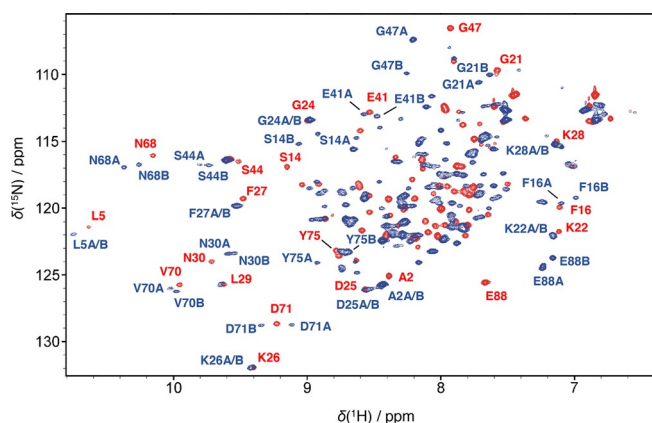


Figure 2. Assigned ¹H,¹⁵N HSQC spectra of S100A4dC (red) and the complex of S100A4dC with unlabeled MPT (blue) at 700 MHz and 300 K. The homodimer becomes asymmetric upon MPT binding, thereby resulting in doubling of resonances (e.g., N68A and N68B are resonances of residue N68 in chains A and B, respectively).

assigned C^α, C^β, C', N and H^N chemical shift values were used for SSP analysis (Figure 3A). We defined an α -helical structure for regions with SSP > 0.5, thus 50% of the conformational ensemble is helical.^[44] On this basis, the four helices are P4–S20 (H1), K31–L46 (H2), D51–S64 (H3), F72–M85 (H4). These results are consistent with secondary structures determined by X-ray crystallography (PDB IDs: 2Q91,^[10] 3C1V,^[11] 3CGA,^[12] 4HSZ).^[14] Loops L1 (containing the pseudo EF1-hand) and L3 (canonical EF2-hand) show some turn property, whereas the hinge loop L2 appears unstructured.

The complex exhibited doubled peaks in the ¹H,¹⁵N HSQC spectrum, compared to free S100A4dC (Figure 2). The reason is the asymmetry of the two monomer chains (A and B) because of complex formation between the symmetric dimer and a single MPT peptide. Our assignments for the complex remained ambiguous for a few residues (M1–L5, E23–K28, and P43), thus linking of these regions has some uncertainty. However, our conclusions were strengthened by the assignments of Elliott

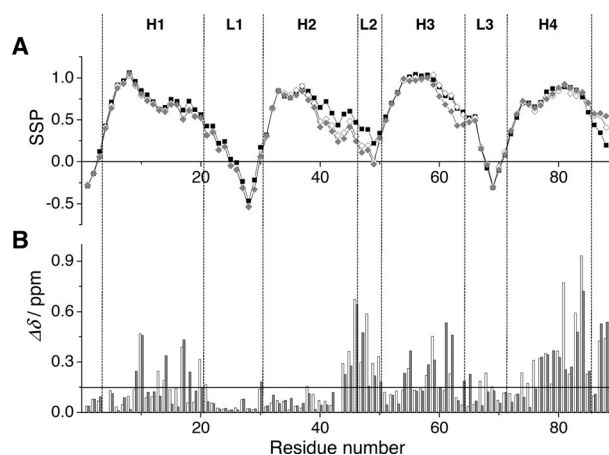


Figure 3. A) SSP scores of free S100A4dC (■) and MPT-bound S100A4dC (◇ and ◆: chains A and B, respectively) along the amino acid sequence. B) Cumulative $\Delta\delta$ chemical shift changes of S100A4dC peaks upon MPT binding (□ and ■ for chains A and B, respectively).

et al., and in several ambiguous cases we relied on their data.^[26] The SSP analysis of the complex (Figure 3A) revealed four helical regions: H1 (P4–S20 in both chains), H2 (K31–T39 in both chains), H3 (D51–D63 in chain A, D51–L62 in chain B), and H4 (F72–E88 in both chains). We note that even though the overall structure is not considerably different from that of the peptide-free S100A4dC, SSP values were lower for H2 in both chains (R40–L46: 0.2–0.5), thus indicating a slight loosening of the structure. There were also slight increases in the SSP values for H4 (M85–E88). For an in-depth examination of both ¹H and ¹⁵N chemical shift changes, cumulative $\Delta\delta$ values were calculated for each residue [Eq. (1)]:^[45]

$$\Delta\delta = \sqrt{[\delta(\text{H}_{\text{complex}}) - \delta(\text{H}_{\text{free}})]^2 + \{0.1[\delta(\text{N}_{\text{complex}}) - \delta(\text{N}_{\text{free}})]\}^2} \quad (1)$$

The changes in chemical shift were higher in the C-terminal region for both chains (Figure 3B). The residues with the highest $\Delta\delta$ (>0.35) were mostly at the canonical binding pockets (L42, F45, L46, K48, M59, F78, S80, C81, A83, M84, N87, E88 in chain A; L46, G47, F55, N61, L62, L79, A83, M84, N87, E88 in chain B), as expected, but interestingly, complex formation also significantly affected residues in H1 (D10, H17 in chain A; D10, S14, H17 in chain B), although this region is further from the interaction surface, and forms part of the dimer interface (Figure S3A and B).

Analysis of ¹⁵N-NMR relaxation measurements

High mobility of MPT. Backbone dynamics can reveal inherent helical motifs in disordered proteins. From the measured ¹⁵N relaxation parameters (T_1 , T_2 relaxation time constants and the ¹H,¹⁵N heteronuclear NOE), reduced spectral density analysis was used for the evaluation of dynamics (Figure 1C).^[46,47] Residues with low $J(0)$ values have the highest mobility; this was obvious for both N- and C-terminal segments, whereas the most rigid part of the molecule was the A1903–G1924 seg-

ment. Temperature dependence of the relaxation parameters (283–298 K) showed that all residues tend to have lower $J(0)$ at higher temperature; the system was highly dynamic at room temperature (Figure S1C), as clearly observable for A1907 (Figure 1D). Thus, as expected, MPT appears to be a highly disordered peptide prior to binding to S100A4dC at room temperature.

H-exchange with the solvent can be monitored by the CLEANEX approach.^[48] H-exchange was effective in the R1912–D1925 region (C-terminal part), in agreement with the hydrophilic character of the molecule (Figure S2). The hydrophobic region of the peptide remained hindered even at higher temperatures.

Comparison of free and MPT-bound S100A4dC behavior. We investigated backbone dynamics by measuring ^{15}N relaxation rates ($1/T$) at 300 K. For S100A4dC these were relatively uniform throughout the entire backbone (0.8 – 1.2 s^{-1} for R_1 , 15 – 20 s^{-1} for R_2 , 15 – 22 for the R_2/R_1 ratio, and 0.7 – 0.9 for the $^1\text{H},^{15}\text{N}$ NOE values; Tables S1, S3, Figure 4). All these relaxation data show that apart from the N and C termini of the molecule the hinge loop L2 has much higher mobility than other regions. This correlates well with the behavior of other S100 proteins: in Ca^{2+} -bound S100A5 a similar relaxation pattern in terms of R_1 , R_2 , R_2/R_1 , and $^1\text{H},^{15}\text{N}$ NOE values was detected.^[31] In our case, however, H1 had an interesting behavior, with slightly lower R_1 and higher R_2 values than the other helices, but no noticeable difference in NOE data. This phenomenon is explained below by Lipari–Szabó model-free formalism.

For the S100A4dC:MPT complex the relaxation rates were 0.7 – 1.1 s^{-1} for R_1 , 14 – 21 s^{-1} for R_2 , 18 – 30 for the R_2/R_1 ratio,

and 0.7 – 0.9 for the $^1\text{H},^{15}\text{N}$ NOE (Tables S2 and S3, Figure 4). As a consequence of the asymmetric binding, differences could be detected between the originally symmetric two subunits (chains A and B), especially in regions L2, L3, and H3.

Protein dynamics analysis by Lipari–Szabó model-free formalism

In order to detect motions on both pico/nanosecond and sub-millisecond timescales and to be able to estimate thermodynamic data, the relaxation results were further analyzed by the extended Lipari–Szabó formalism method.^[49–52] We used the FAST-Modelfree^[53] program^[54,55] with the measured R_1 , R_2 and $^1\text{H},^{15}\text{N}$ NOE values for each residue to fit the following parameters: generalized order parameter (S^2), global rotational correlation time (τ_c), correlation time for internal motion (τ_e) and the exchange parameter (R_{ex}) to describe chemical or conformational exchange processes.

The isotropy of the molecules was estimated from X-ray structures with the program HYDROPRO.^[56] The ratios of the three eigenvalues of the rotational diffusion tensor were $1.30:1.15:1.00$ for S100A4dC (PDB ID: 2Q91)^[10] and $1.25:1.11:1.00$ for the S100A4dC:MPT complex (PDB ID: 3ZWH).^[25] As approximated rotational diffusion tensor anisotropy ratios (D_{\parallel}/D_{\perp}) were in the 0.77 – 0.90 range, we concluded that for both molecules the axially anisotropic approach can be applied in dynamics analysis.

Throughout the calculations, amide N–H bond lengths were set to 1.02 \AA , and -172 ppm was taken as the ^{15}N chemical shift anisotropy.^[57] NMR structures (PDB ID: 2MRD for

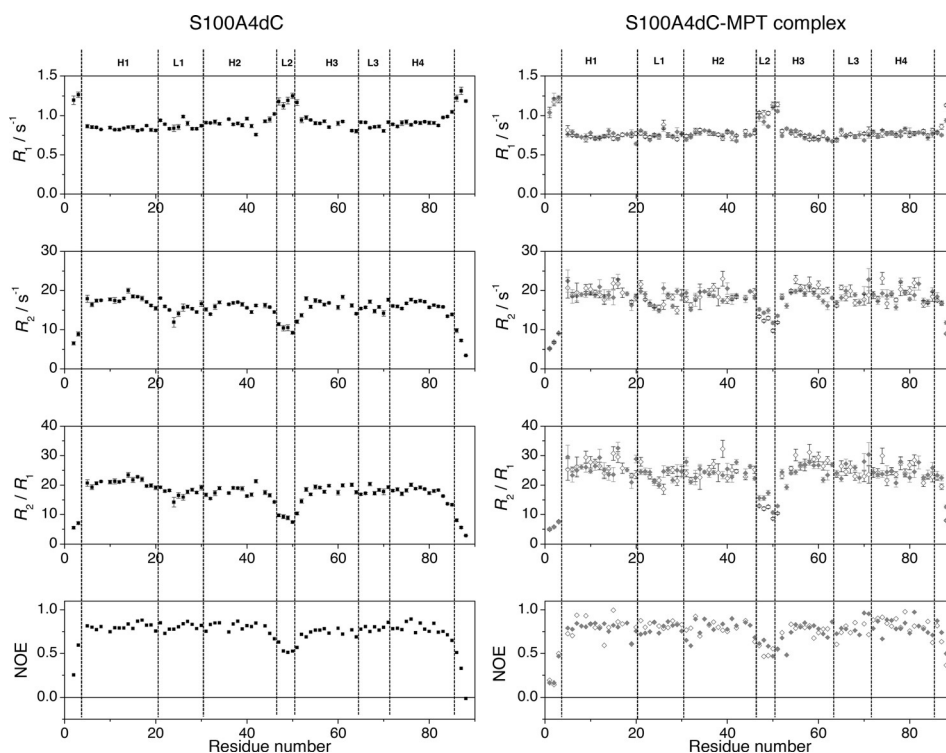


Figure 4. ^{15}N relaxation data of the Ca^{2+} -bound S100A4dC (\blacksquare) and the S100A4dC:MPT complex (\diamond and \blacklozenge : chains A and B, respectively) at 300 K (R_1 , R_2 , R_2/R_1 , and $^1\text{H},^{15}\text{N}$ NOE). Vertical lines delineate major secondary structure elements of S100A4.

S100A4dC,^[13] 2LNK for S100A4dC:MPT^[26]) were used for rotational diffusion tensor calculation; for the purpose of comparison with our results, residues 89–101 were deleted from the C-terminal tail before fitting. Due to peak overlapping, the following residues were omitted from the calculation: M1, L9, K35, M59, and L62 (S100A4dC), A8, K18, K35, F45, A53, D63, E69, and I82 (S100A4dC:MPT chain A), and L38 and D67 (S100A4dC:MPT chain B). There was no assigned peak for H17 of chain B of the complex. No model could be fitted for residues S32, E52, and I82 (S100A4dC), G24 (S100A4dC:MPT chain A) or D25, S32, and A53 (S100A4dC:MPT chain B; Tables S4 and S5).

The calculated global rotational correlation time values were 11.31 ± 0.01 ns (S100A4dC) and 13.42 ± 0.03 ns (S100A4dC:MPT). These data are in good agreement with the approximated values obtained from the R_2/R_1 ratios^[58] (11.44 ns (S100A4dC) and 13.35 ns (S100A4dC:MPT)) and with data obtained for similarly sized proteins. Other S100 family members showed 9.12–13.52 ns after recalculation to 300 K.^[28–30,34,35,59]

The calculated D_{\parallel}/D_{\perp} ratios were 0.91 ± 0.01 (S100A4dC) and 0.93 ± 0.01 (S100A4dC:MPT); thus, our experimentally obtained values were very close to the anisotropies calculated in HYDROPRO (fitted parameters for each residue in Figure 5, Tables S4 and S5).

The S^2 order values (apart from the highly mobile N- and C-terminal tails) were 0.46–0.97 and 0.41–0.96 for Ca^{2+} - and peptide-bound proteins, respectively. These data are in accordance with the result of the structural observation: the whole molecule (except the L2 hinge) had noticeable rigidity, both in the absence and presence of the peptide ligand, and interestingly, MPT binding did not substantially influence the global internal mobility of the protein backbone. The same results were obtained when comparing the relaxation derived S^2 values with the predicted values derived from chemical shifts by using the random coil index (RCI,^[59] Figure 5A). However, an interesting and unexpected observation was the appearance of R_{ex} values for several residues in the peptide-free S100A4dC, mostly in H1 (Figure 5C).

This indicates slow motions in H1 (micro- to millisecond timescale), an interesting finding, as this is part of the X-type H1–H4–H1'–H4' bundle that stabilizes the dimer. Moreover, upon complex formation this slow motion component disappeared (Figure 5D), with only a few nonzero R_{ex} residues in H1. Fast internal mobility demonstrated by τ_e values were found not only in N- and C-terminal tails but also in the L2 loops, thus indicating substantial flexibility of the hinge regions, both in free S100A4dC and in the complex. We also tried to detect the conformational exchange by CPMG relaxation dispersion measurements, which report micro- to millisecond motions. Values were obtained in H1, H4, and L2 (Figure 5C). The discrepancy between the measured and determined R_{ex} contributions arises from the fact that different timescales were tested by the two approaches. However, no R_{ex} contribution was detectable in the complex (data not shown), in accordance with the Lipari–Szabó analysis. This means that H1 and H4 exhibit slow conformational motion, which is restricted upon peptide binding (Figure S3C).

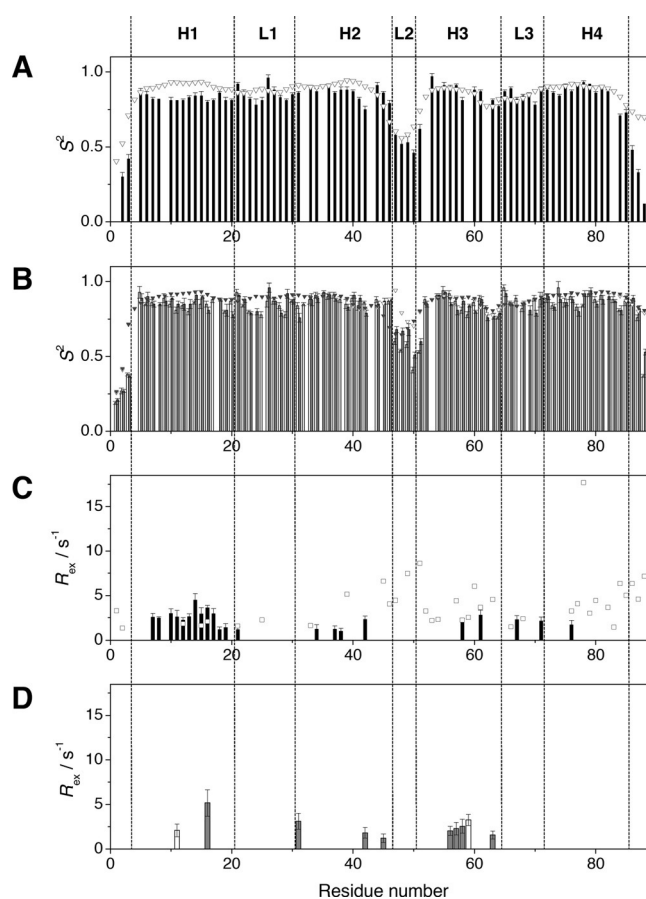


Figure 5. Fitted S^2 and R_{ex} parameters by Lipari–Szabó model-free analysis for (A) and (C) S100A4dC (■) and (B) and (D) S100A4dC:MPT (◇ and ◆; values for chains A and B, respectively). S^2 order parameters predicted from RCI values are shown as triangles in (A) and (B); □: measured R_{ex} parameters derived from CPMG measurements in (C).

Thermodynamic aspects: entropic contribution from the backbone. The overall entropy change for a system upon complex formation is given by the sum of the changes in conformational, hydration, and rotational-translational entropies of the interacting partners (S100A4dC and MPT) given by Equation (2):

$$\Delta S_{\text{overall}} = \Delta S_{\text{conf}} + \Delta S_{\text{hydr}} + \Delta S_{\text{rot-trans}} \quad (2)$$

where ΔS_{conf} is composed of entropy changes in the backbone and the side-chains [Eq. (3)]:

$$\Delta S_{\text{conf}} = \sum \Delta S_i^{\text{bb}} + \sum \Delta S_i^{\text{sc}} \quad (3)$$

where ΔS_i^{bb} and ΔS_i^{sc} are the entropy changes of the backbone and side-chain, respectively, of a particular residue. For estimation of the S100A4dC value of ΔS_i^{bb} , the calculated generalized order parameters for individual N–H bonds were used [Eq. (4)].^[61]

$$\Delta S_i^{\text{bb}} = R \ln \left\{ \frac{[3 - (1 + 8S_{i,\text{complex}})^{1/2}]/[3 - (1 + 8S_{i,\text{free}})^{1/2}]}{[3 - (1 + 8S_{i,\text{free}})^{1/2}]} \right\} \quad (4)$$

where ΔS_i^{bb} is the conformational entropy change of one N–H bond vector, S_i is the square root of the fitted generalized

order parameter S_i^2 of the given bond vector of the individual residue, and R is the universal gas constant (calculated values for each secondary structure element in Figure S4 and Table 1). The negative tendency was most pronounced for H1, thus indicating that this is the region with substantially increased rigidity upon MPT-binding. The calculated overall $\Sigma\Delta S_i^{bb}$ value was $-168.3 \text{ J mol}^{-1} \text{ K}^{-1}$; the negative sign predicts ordering of the backbone after binding. In conclusion, the contribution from S100A4dC conformational changes to the $-T\Delta S_{\text{conf}}$ conformational entropic cost at 300 K was $+50.49 \text{ kJ mol}^{-1}$. The experimentally determined overall entropic contribution obtained from ITC measurements for the same S100A4dC complex was $+17.2 \text{ kJ mol}^{-1}$.^[27] This means hydration and rotational–translational terms as well as all terms arising from S100A4 side chains and from MPT must be considerably larger, in order to compensate for the difference. This is not surprising given that entropy values from different sources (conformational, hydration, rotational–translational) show a very wide range relative to one another in other protein complexes.^[62]

Comparison of dynamics among S100 proteins

The dynamics of several S100 proteins have been investigated with the Lipari–Szabó model-free approach. Data are available for apo-S100A1 in free form and modified by β -mercaptoethanol,^[28,29] Ca^{2+} -S100A1 and its homocysteine thionylated form (Hcy),^[35] apo-S100B,^[34] and apo-S100A4.^[30] We compared these results with our data for Ca^{2+} -bound S100A4dC and the S100A4dC:MPT complex.

For L1 and L3 accommodating EF1- and EF2-hands (S100A1 and S100A4), binding of Ca^{2+} resulted in significant increases in rigidity, as determined from the averaged generalized order parameters (Table 1), where a 0.2–0.3 increase in the corresponding S^2 values was detected. This is obviously a result of formation of new bonds upon Ca^{2+} coordination in these regions. Interestingly, apo-S100B already had high S^2 values in both L1 and L3, thus suggesting that these regions are as rigid in Ca^{2+} -S100B as in the apo form. This can be explained by an

antiparallel alignment with hydrogen bonds of the two small β -strands in the loops, thus bringing the EF1- and EF2-hands together.^[37] These structural elements are missing in apo-S100A1 and apo-S100A4.

The hinge region (L2) is much more flexible in both apo and Ca^{2+} -bound S100A4 than in any other S100 protein. This flexibility is supported by the existence of fast timescale motions reflected in the τ_e values. Regarding the behavior of the four helices, those of S100A1 were the most rigid, whereas S100B had the most flexible helices (S100A4 was in between).

Slow-timescale motions characterized by the R_{ex} conformational exchange parameter were detected for H1 residues in apo- and Ca^{2+} -S100B, as well as in apo- and Ca^{2+} -S100A4. The most significant variation was observed in the S100A4 system. In the apo form, the R_{ex} contribution was mainly in the EF1-hand, in the L2 loop, a few residues in the EF2-hand, and the tail region (missing in S100A4dC).^[30] In the Ca^{2+} -bound form (our present study) these residues lack the R_{ex} term, whereas this motion was present in 25% of the H1 residues. Moreover, in the complex with MPT the residues characterized by R_{ex} were dramatically reduced (3.4% in chain A; 9.1% in chain B), thus meaning restriction of this slow-timescale conformational motion in the presence of the peptide. A similar disappearance of R_{ex} terms in the target-bound protein was observed for Ca^{2+} -bound S100B when interacting with a 12-residue peptide (TRTK).^[37]

Comparative approach with protein dynamics and X-ray crystallography B-factors suggests different behavior of the EF-hands

Solution NMR studies reveal pico-/nanosecond timescale motions. These motions are also present in the solid (crystal) state. Correlation of the NMR-derived order parameters (S^2) with the B-factor data obtained from X-ray crystal structures has been attempted;^[63] generally the lower the S^2 value (i.e., the more mobile the region), the higher the B factor. S^2 values can be calculated directly from relaxation data (as shown previ-

Table 1. Average generalized order parameters in various S100 proteins calculated for each structural element (helices H1–H4 and loops L1–L3) and for Ca^{2+} -coordinating residues in the EF hands.

Protein state organism	S100A4	S100A4-MPT		S100A4	S100B	S100A1	S100A1- β ME	S100A1	S100A1	S100A1-Hcy
	Ca^{2+} -bound human	chain A Ca^{2+} -bound human	chain B Ca^{2+} -bound human	apo murine	apo human	apo bovine	apo bovine	apo human	Ca^{2+} -bound human	Ca^{2+} -bound human
Ref.				[30]	[34]	[28]	[28]	[29]	[35]	[35]
H1 helix	0.83	0.85	0.86	0.89	0.87	0.86	0.92	0.92	0.90	0.91
L1 loop	0.85	0.84	0.87	0.61	0.82	0.85	0.78	0.76	0.95	0.91
H2 helix	0.86	0.87	0.87	0.84	0.86	0.83	0.90	0.91	0.91	0.85
L2 loop (hinge)	0.52	0.53	0.63	0.63	0.84	0.86	0.85	0.87	0.82	0.58
H3 helix	0.85	0.84	0.82	0.77	0.84	0.95	0.91	0.87	0.88	0.84
L3 loop	0.85	0.87	0.84	0.57	0.78	0.90	0.82	0.75	0.82	0.88
H4 helix	0.86	0.88	0.87	0.91	0.87	0.90	0.93	0.92	0.95	0.95
EF 1 hand ^[a]	0.83	0.83	0.81	0.66	0.83	0.83	0.87	0.79	0.92	0.92
EF 2 hand ^[b]	0.84	0.94	0.85	0.60	0.78	0.87	0.90	0.81	0.95	0.89

[a] Ca^{2+} -binding residues: S20, E23, D25, K28 and E33 [b] Ca^{2+} -binding residues: D63, N65, D67, E69, and E74.

ously), and can also be predicted on the basis of chemical shift values. S^2 values obtained by these two NMR-based methods for Ca^{2+} -bound S100A4dC are in Figure 5A. Discrepancies are evident in H1, as the values are distinct for residues representing slow conformational changes, thus suggesting that the prediction approach cannot detect this property; differences were also observed in the mobile regions. Analyzing the changes in the NMR-based S^2 values (Tables 1, S4 and S5) for the Ca^{2+} -coordinating residues of the two EF-hands in free and MPT-bound S100A4dC, we observed that the data were similar for the EF1-hand in chain A, whereas S^2 values in chain B were lower (correlating with increased mobility). For the EF2-hand an increase in S^2 in chain A was observed, thus indicating increased rigidity; almost no variation was detected in chain B (Figure S3C).

These findings correlate with the changes in B-factors for PDB structures 3CGA and 3ZWH by the approach of Liriano et al.^[37] For each residue the B factors for all atoms were averaged, and the resulting (specific) values of all amino acid residues were further averaged. Finally, the difference between the specific and global average values was plotted against residue number. The analysis showed that the EF1-hand of chain B is more flexible in the complex, whereas this mobility increase is only partial in the EF2-hand (Figure 6). On the other hand, the EF2-hand of chain A is more rigid in the complex, and there are only slight changes in the EF1-hand. These results are consistent with conclusions obtained from NMR dynamics, and the presented comparisons indicate that both methods detect variations in the dynamic features of Ca^{2+} -binding residues, with a clear distinction between EF1- and EF2-hand properties. This finding certainly contributes to an explanation for the high Ca^{2+} affinity of MPT-bound S100A4. The higher Ca^{2+} affinity of the S100B:TRTK complex (even though only fivefold,^[37] compared to 10 000-fold^[26] for S100A4:NMIIA) correlates with the decrease in the rigidity of the EF2-hand. In our case, a similar mobility decrease in the Ca^{2+} -binding residues

in the EF2-hand of chain A was observed; moreover, there are contributions from other detected dynamic features, such as the disappearance of slow motions in the dimer interface (represented by R_{ex}). Even though the changes in dynamics were not dramatic, these multi-level allosteric effects were the only observed differences in the properties of the complex compared to peptide-free protein to account for the elevated Ca^{2+} affinity.

Preformed α -helix in MPT can be important in the mechanism of complex formation between S100A4 and NMIIA

Two main mechanisms have been proposed for the folding of intrinsically disordered protein segments upon binding to a folded partner protein: 1) the conformational selection model, and 2) the induced-folding model.^[64–66] Our results indicate that during complex formation between S100A4 and MPT, the first mechanism is more probable, as the inherent helicity of the MPT central region is perfectly accommodated in the S100A4 site formed by H3 and H4, prone to bind an α -helical target of up to 16 residues.^[14,27,43] Note that this helix is part of the C-terminal coiled-coil of NMII tail, therefore it should be “unzipped” to be available for S100A4 binding. The preformed helix observed in MPT could mean that the coiled-coil helix does not completely unfold during unzipping of the dimer NMII tail, thus decreasing the entropic cost of complex formation and contributing to the extremely high affinity of the complex ($K_d \approx 0.1 \text{ nM}$).^[27] Comparing S100A4 binding to NMII isoforms, we recently showed that the major determinant of isoform-specific complex formation is A1907. In both NMIIA and NMIIIC, this residue is at the N-terminal end of the region containing the nascent helix found in our present NMR studies, a helix that forms a central modular element in the allosteric interacting network of complex formation.^[67]

Increased Ca^{2+} affinity of S100A4:NMIIA complex is induced by dynamics rather than structural changes

It is well known that for many EF-hand proteins, Ca^{2+} binding affinity is low unless bound to the biological target.^[37,68] The Ca^{2+} affinity for most S100 proteins is in the micromolar range, whereas in the presence of the interaction partner (TRTK-12 for S100B,^[37] RyR for S100A1),^[40] this value can increase up to 300-fold. In the case of S100A4, binding to NMIIA is accompanied by an increase of at least four orders of magnitudes in Ca^{2+} affinity (the microscopic K_d values for the EF2-hand are $5 \mu\text{M}$ and 0.5 nM , for apo and peptide-bound S100A4, respectively).^[26] The reasons and factors influencing the increased Ca^{2+} affinity can be explained by three possible model mechanisms.^[37]

In model 1 (the most straightforward), discrete structural changes have the effect of changing from a weaker Ca^{2+} coordination geometry to a more optimal one. Our structural observations based on the chemical shifts showed no change for either EF-hand, and this was reinforced by the very similar average order parameter values for L1 and L3 (Table 1). Moreover, the X-ray structures show no detectable changes in the

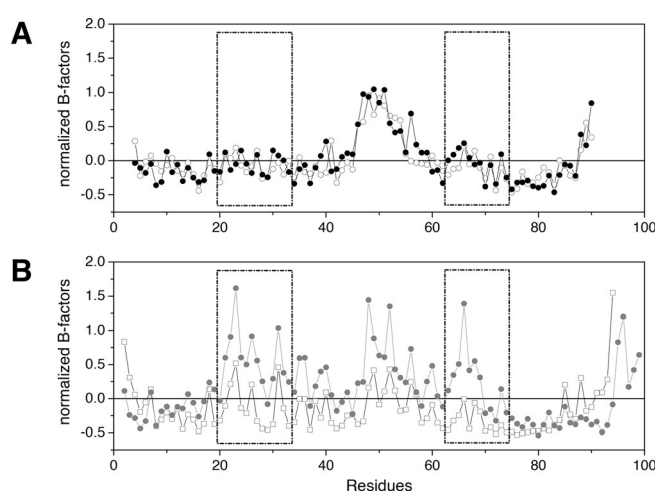


Figure 6. Normalized B-factors calculated according to Liriano et al.^[37] for X-ray structures: A) S100A4 (PDB ID: 3CGA);^[12] ○ and ●: chains A and B, respectively; B) S100A4:MPT (PDB ID: 3ZWH);^[25] ○ and ●: chains A and B, respectively. EF1- and EF2-hands are boxed.

Ca²⁺-coordination sphere (Figure S5). In the case of S100B, no structural changes were detected either; however, dynamic motions in the EF2-hand Ca²⁺-coordinating residues were stabilized upon TRTK-12 binding.

Model 2 is based on a pre-equilibrium between closed (prior to Ca²⁺ binding) and open (Ca²⁺-bound) states. Earlier studies showed no evidence of MPT binding in the absence of Ca²⁺.^[10] Backbone dynamics studies conducted on murine apo-S100A4^[30] showed slow conformational motions characterized by R_{ex} values in several parts of the EF1-hand region but barely in the EF2-hand (also in L2 and at the C terminus, which is missing in our deletion mutant). Upon Ca²⁺ binding, both H4 and L2 were affected. The dynamics of the Ca²⁺-bound protein, however, did not exhibit any slow motion at the Ca²⁺-coordination sites. This implies that the pre-equilibrium model is unlikely to apply in this case either. Our results for S100A4dC showed no R_{ex} values in the Ca²⁺ binding positions; they were mostly in H1. These results indicate that there is no chemical exchange between the open and close states for the Ca²⁺-bound protein prior to target binding.

Model 3 ("target binding and functional folding")^[1,37] is based on pre-equilibrium conformational averaging between Ca²⁺ binding states with different affinities in the absence of the peptide target. This is a conformational selection-type mechanism: induced-fit transition from a closed (apo) to an open (Ca²⁺-bound) state, where binding of the interaction partner shifts the open state towards higher-affinity Ca²⁺-binding substates with attenuated dynamic features throughout the protein. Even though our analysis did not conclude slow-timescale motions in the EF hands, the slow conformational motion of H1 disappeared in the MPT-bound form, the H2 content slightly decreased, the H4 content slightly increased, and the structure loosened for L2; finally, target binding made the whole backbone slightly more rigid (as evidenced by the decrease in conformational entropy). Therefore we conclude this model is the best suited to explain the observed changes in dynamics.

Changes in dynamics of H1 can contribute to increased dimer stability of the complex

Based on the SSP scores, the major secondary-structure elements of S100A4 were conserved upon MPT binding. The changes mostly affected H2, the structure of which loosened significantly, and a small extension of H4 was detected. The most pronounced chemical shift variations were concentrated at the binding region, as expected, but interestingly, residues at the inward-facing part of H1 also showed significant variation. As H1 is not directly involved in peptide binding, perturbations in the environment are a consequence of allosteric conformational variations when the peptide ligand binds. This particular behavior of H1 is supported by the dynamic measurements, as slow conformational motions were found in free S100A4dC but not in the complex. A plausible explanation based on relaxation data is that the complex is characterized by a more-rigid structure, thereby causing loss of conformational exchange. Significant changes in chemical shifts were

detected in this region as well. Our analysis shows that complex formation affects not only the binding site of S100A4 but also other structural elements (specifically, H1 in the X-type four-helix bundle subunit interface), by an allosteric mechanism. Changes in the dynamic properties of H1 might be associated with a change in S100A4 dimer stability, which is thought to be relatively low ($K_d = 4 \mu\text{M}$).^[69] Because Ca²⁺ binding promotes dimerization,^[69] thermodynamic coupling also requires an increase in dimer stability upon target binding, and changes in the dynamics of some H1 residues could provide a mechanism for this allosteric regulation. Alternatively, H1 rigidity together with variations in mobility of the EF-hands could contribute to the increased stability and the increased Ca²⁺ affinity of peptide-bound S100A4. R_{ex} was also detected in H1 of S100B, and this was eliminated upon target peptide binding,^[37] however, this dynamic change is unlikely to affect dimer stability, which is very high even in the peptide-free protein ($K_d < 1 \text{ nM}$).^[70]

Conclusion

We have shown that no significant structural alteration occurs upon complex formation of Ca²⁺-bound S100A4dC with the NMIIA peptide MPT; therefore, changes in protein dynamics are concluded to be the only reasons to explain the large increase in Ca²⁺ affinity in the presence of the interacting partner, and possibly also an increase in dimer stability. These changes were detected both globally and locally: the backbone of S100A4 becomes slightly more ordered and, locally, the contribution of H1 is significant, as evidenced by the disappearance of slow conformational exchange upon complex formation. This effect is surprising considering that H1 is far from the peptide-interacting surface. A decrease in the dynamics of H1 might also contribute to dimer stabilization in the complex. Ca²⁺-binding residues of EF1- and EF2-hands show altered dynamics in the two identical chains of the homodimer, as a result of the asymmetric binding of MPT. Increased mobility of the EF1-hand in chain B and rigidity of the EF2-hand in chain A was observed.

In summary, the functional sites of this small Ca²⁺-binding protein apparently communicate with each other by an allosteric network that operates with multilevel changes in protein dynamics. We propose that these changes in dynamics contribute significantly to the conformational adaptation that enables the vertebrate-specific S100A4 to fine-tune protein-protein interactions, similarly to dynamics changes suggested previously for target recognition in calmodulin.^[71,72]

Our results are in agreement with findings for the S100B family member. Ca²⁺-bound S100B also exhibits dynamics on multiple timescales, and these are eliminated upon binding of an interaction partner. The target-bound conformation is more stable and more rigid, and this contributes to the increase in Ca²⁺ affinity. This information is crucial to developing and testing therapeutic inhibitors, which must also mimic the stabilizing effect of the protein-interaction partners on conformational dynamics.^[73]

Experimental Section

Protein expression and purification: His-tagged human S100A4 (UniProt accession no. P26447) and the 45-residue NMIIA (UniProt accession no. P35579) fragment R1893Y–K1937 were expressed and purified as previously described.^[25] The expression of ¹³C- and/or ¹⁵N-labeled proteins was modified as follows. *Escherichia coli* BL21(DE3) cells carrying the plasmid encoding S100A4dC or NMIIA fragment were grown in lysogeny broth (LB, 1 L) at 37 °C until the OD₆₀₀ reached 0.8. The cells were harvested by centrifugation, washed thoroughly with sterile phosphate-buffered saline solution (PBS) and resuspended in PBS (1 L) supplemented with ¹⁵NH₄Cl (1 g) and/or ¹³C-glucose (2 g), CaCl₂ (0.1 mM), and MgSO₄ (2 mM). After shaking for 30 min at 37 °C, protein expression was induced with IPTG (0.5 mM) for 4 h at 37 °C.

NMR experiments: Measurements were performed on an Avance III 700 MHz spectrometer (Bruker) equipped with a z-gradient 5 mm probe-head, an Avance III 900 MHz spectrometer equipped with a cryoprobe, and an Avance 700 MHz spectrometer with a TXO cryoprobe, operating at 700.13, 898.56, and 700.06 MHz, respectively (¹H), 176.06, 225.94, and 176.03 MHz, respectively (¹³C), and 70.94, 91.05, and 70.93 MHz, respectively (¹⁵N). The temperature range for MPT studies was 283–310 K, and temperature was calibrated by standard glycol and methanol solutions. Typical composition of the NMR sample for MPT backbone and side-chain assignment was: ¹⁵N- or ¹³C-/¹⁵N-labeled protein (1 mM), 2-(*N*-morpholino)ethansulfonic acid (MES) buffer (10 mM, pH 5.4–6.2), NaCl (20 mM), TCEP (tris-(2-carboxyethyl)phosphine hydrochloride; 10 mM), Na₂S₂O₃ (3 mM), and D₂O (10%). For S100A4dC the composition was similar, but with CaCl₂ (10 mM). The MPT:S100A4dC samples contained unlabeled MPT (2 mM), and ¹³C-/¹⁵N-labeled S100A4dC (1 mM). All chemical shifts were referenced to the internal DSS resonance; ¹³C, ¹⁵N chemical shifts were referenced indirectly from the corresponding gyromagnetic ratios according to IUPAC convention.

Sequence-specific assignment of H^N, N, C', C^α, C^β and further side-chain resonances was done on the basis of HNCA, HN(CO)CA, HNCACB, (H)CC(CO)NH, HNCO, HSQC-TOCSY, HSQC-NOESY (700 and 900 MHz), BEST-HNCACB (900 MHz), CON, CACO (700 MHz TXO) measurements. MPT temperature dependence was assessed from the ¹H, ¹⁵N HSQC spectra. MPT was investigated at 283 K; characterization of S100A4dC and the complex was performed at 300 K. All spectra were processed with TOPSPIN and analyzed in CARA (ETH Zürich, <http://wiki.cara.nmr.ch/>)^[74] and SPARKY.^[75] The assigned chemical shifts have been deposited in the Biological Magnetic Resonance Data Bank (entries 25992 (MPT), 25136 (S100A4dC), 25208 (S100A4dC:MPT)).

For dynamics studies, *T*₁, *T*₂, steady-state heteronuclear ¹H, ¹⁵N NOE, CLEANEX, and relaxation dispersion measurements on [¹⁵N]S100A4dC and unlabeled MPT–[¹⁵N]S100A4dC complex were measured on the Avance III 700 MHz spectrometer with standard Bruker pulse sequences at 300 K. A typical spectrum was recorded over 0.005–2.8 s for *T*₁ and 0.017–0.508 s for *T*₂. The longitudinal (*R*₁) and transverse (*R*₂) relaxation rates were determined by fitting the crosspeak intensities as a function of the delay to a single-exponential decay in SPARKY.^[75] Heteronuclear NOE values were obtained from the ratio of the peak intensities of saturated and unsaturated crosspeaks, and CLEANEX evaluation was done in a similar manner. Relaxation dispersion spectra were recorded as a series of 14 2D data sets with B1 field strengths *v*_{CPMG} in the 25–1000 Hz range, with repeat experiments at 200 and 800 Hz. A reference

spectrum omitting the CPMG interval was also recorded. Data analysis was performed with Dynamics center software (Bruker).

Backbone relaxation data were further analyzed by the FAST-Modelfree^[53] (Facile Analysis and Statistical Testing for Modelfree), the automated version of Modelfree 4.2 software.^[54,55]

Acknowledgements

Fruitful discussions with Prof. Gyula Batta and Prof. András Perczel are highly acknowledged. We thank Dr. Gergő Horváth for his initial help with the Modelfree program. Financial support by the Hungarian National Research Fund (OTKA) grants K108437, NK 101072; the MedInProt; and from the Access to the Bio-NMR Research Infrastructure (at CERM, Florence, Italy) co-funded under the 7th Framework Program of the EC (FP7/2007–2013) grant agreement 261863 for conducting the research are gratefully acknowledged. The European Union and the European Social Fund have provided financial support to the project under Grant Agreement TÁMOP 4.2.1/B-09/KMR-2010-0003 and the TÁMOP 4.2.4. A/1-11-1-2012-0001 "National Excellence Program".

Keywords: backbone dynamics • Ca²⁺ affinity • NMR spectroscopy • protein–protein interactions • S100A4 protein

- [1] A. R. Bresnick, D. J. Weber, D. B. Zimmer, *Nat. Rev. Cancer* **2015**, *15*, 96–109.
- [2] I. Marenholz, C. W. Heizmann, G. Fritz, *Biochem. Biophys. Res. Commun.* **2004**, *322*, 1111–1122.
- [3] K. Boye, G. M. Mælandsmo, *Am. J. Pathol.* **2010**, *176*, 528–535.
- [4] B. R. Davies, M. P. Davies, F. E. Gibbs, R. Barraclough, P. S. Rudland, *Oncogene* **1993**, *8*, 999–1008.
- [5] S. R. Jenkinson, R. Barraclough, C. R. West, P. S. Rudland, *Br. J. Cancer* **2004**, *90*, 253–262.
- [6] E. Lukanidin, J. P. Sleeman, *Semin. Cancer Biol.* **2012**, *22*, 216–225.
- [7] S. K. Mishra, H. R. Siddique, M. Saleem, *Cancer Metastasis Rev.* **2012**, *31*, 163–172.
- [8] L. Huang, Y. Xu, G. Cai, Z. Guan, S. Cai, *Oncol. Rep.* **2012**, *27*, 917–922.
- [9] K. M. Vallely, R. R. Rustandi, K. C. Ellis, O. Varlamova, A. R. Bresnick, D. J. Weber, *Biochemistry* **2002**, *41*, 12670–12680.
- [10] V. N. Malashkevich, K. M. Varney, S. C. Garrett, P. T. Wilder, D. Knight, T. H. Charpentier, U. A. Ramagopal, S. C. Almo, D. J. Weber, A. R. Bresnick, *Biochemistry* **2008**, *47*, 5111–5126.
- [11] A. R. Gingras, J. Basran, A. Prescott, M. Kriajevska, C. R. Bagshaw, I. L. Barsukov, *FEBS Lett.* **2008**, *582*, 1651–1656.
- [12] P. Pathuri, L. Vogeley, H. Luecke, *J. Mol. Biol.* **2008**, *383*, 62–67.
- [13] C. C. Cho, K.-W. Hung, D. R. Gorja, C. Yu, *J. Biomol. NMR* **2015**, *62*, 233–238.
- [14] U. A. Ramagopal, N. G. Dulyaninova, K. M. Varney, P. T. Wilder, S. Nallamsetty, M. Brenowitz, D. J. Weber, S. C. Almo, A. R. Bresnick, *BMC Struct. Biol.* **2013**, *13*, 31.
- [15] Y. Watanabe, N. Usada, H. Minami, T. Morita, S. Tsugane, R. Ishikawa, K. Kohama, Y. Tomida, H. Hidaka, *FEBS Lett.* **1993**, *324*, 51–55.
- [16] M. V. Kriajevska, M. N. Cardenas, M. S. Grigorian, N. S. Ambartsumian, G. P. Georgiev, E. M. Lukanidin, *J. Biol. Chem.* **1994**, *269*, 19679–19682.
- [17] K. Takenaga, Y. Nakamura, S. Sakiyama, Y. Hasegawa, K. Sato, H. Endo, *J. Cell Biol.* **1994**, *124*, 757–768.
- [18] M. Kriajevska, M. Fischer-Larsen, E. Moertz, O. Vorm, E. Tulchinsky, M. Grigorian, N. Ambartsumian, E. Lukanidin, *J. Biol. Chem.* **2002**, *277*, 5229–5235.
- [19] M. Grigorian, S. Andresen, E. Tulchinsky, M. Kriajevska, C. Carlberg, C. Kruse, M. Cohn, N. Ambartsumian, A. Christensen, G. Selivanova, E. Lukanidin, *J. Biol. Chem.* **2001**, *276*, 22699–22708.

- [20] A. Semov, M. J. Moreno, A. Onichtchenko, A. Abulrob, M. Ball, I. Ekiel, G. Pietrzynski, D. Stanimirovic, V. Alakhov, *J. Biol. Chem.* **2005**, *280*, 20833–20841.
- [21] S. C. Garrett, K. M. Varney, D. J. Weber, A. R. Bresnick, *J. Biol. Chem.* **2006**, *281*, 677–680.
- [22] Z.-H. Li, A. Spektor, O. Varlamova, A. R. Bresnick, *Biochemistry* **2003**, *42*, 14258–14266.
- [23] Z.-H. Li, A. R. Bresnick, *Cancer Res.* **2006**, *66*, 5173–5180.
- [24] E. J. Kim, D. M. Helfman, *J. Biol. Chem.* **2003**, *278*, 30063–30073.
- [25] B. Kiss, A. Duelli, L. Radnai, K. A. Kékesi, G. Katona, L. Nyitray, *Proc. Natl. Acad. Sci. USA* **2012**, *109*, 6048–6053.
- [26] P. R. Elliott, A. F. Irvine, H. S. Jung, K. Tozawa, M. W. Pastok, R. Picone, S. K. Badyal, J. Basran, P. S. Rudland, R. Barraclough, L.-Y. Lian, C. R. Bagshaw, M. Kriajevska, I. L. Barsukov, *Structure* **2012**, *20*, 654–666.
- [27] A. Duelli, B. Kiss, I. Lundholm, A. Bodor, M. V. Petoukhov, D. I. Svergun, L. Nyitray, G. Katona, *PLoS One* **2014**, *9*, e97654.
- [28] I. Zhukov, A. Ejchart, A. Bierzyński, *Biochemistry* **2008**, *47*, 640–650.
- [29] M. Nowakowski, Ł. Jaremko, M. Jaremko, I. Zhukov, A. Belczyk, A. Bierzyński, A. Ejchart, *J. Struct. Biol.* **2011**, *174*, 391–399.
- [30] K. Dutta, C. J. Cox, R. Basavappa, S. M. Pascal, *Biochemistry* **2008**, *47*, 7637–7647.
- [31] I. Bertini, S. D. Gupta, X. Hu, T. Karavelas, C. Luchinat, G. Parigi, J. Yuan, *J. Biol. Inorg. Chem.* **2009**, *14*, 1097–1107.
- [32] F. Arnesano, L. Banci, I. Bertini, A. Fantoni, L. Tenori, M. S. Viezzoli, *Angew. Chem. Int. Ed.* **2005**, *44*, 6341–6344; *Angew. Chem.* **2005**, *117*, 6499–6502.
- [33] I. Bertini, V. Borsi, L. Cerofolini, S. D. Gupta, M. Fragai, C. Luchinat, *J. Biol. Inorg. Chem.* **2013**, *18*, 183–194.
- [34] K. G. Inman, D. M. Baldisseri, K. E. Miller, D. J. Weber, *Biochemistry* **2001**, *40*, 3439–3448.
- [35] M. Nowakowski, K. Ruszczyńska-Bartnik, M. Budzińska, L. Jaremko, M. Jaremko, K. Zdanowski, A. Bierzyński, A. Ejchart, *Biochemistry* **2013**, *52*, 1149–1159.
- [36] N. T. Wright, K. G. Inman, J. A. Levine, B. R. Cannon, K. M. Varney, D. J. Weber, *J. Biomol. NMR* **2008**, *42*, 279–286.
- [37] M. A. Liriano, K. M. Varney, N. T. Wright, C. L. Hoffman, E. A. Toth, R. Ishima, D. J. Weber, *J. Mol. Biol.* **2012**, *423*, 365–385.
- [38] G. Fanò, S. Biocca, S. Fulle, M. A. Mariggio, S. Belia, P. Calissano, *Prog. Neurobiol.* **1995**, *46*, 71–82.
- [39] E. A. Dukhanina, A. S. Dukhanin, M. Y. Lomonosov, E. M. Lukanidin, G. P. Georgiev, *FEBS Lett.* **1997**, *410*, 403–406.
- [40] N. T. Wright, B. L. Prosser, K. M. Varney, D. B. Zimmer, M. F. Schneider, D. J. Weber, *J. Biol. Chem.* **2008**, *283*, 26676–26683.
- [41] J. Markowitz, R. R. Rustandi, K. M. Varney, P. T. Wilder, R. Udan, S. L. Wu, W. D. Horrocks, D. J. Weber, *Biochemistry* **2005**, *44*, 7305–7314.
- [42] D. B. Zimmer, D. J. Weber, *Cardiovasc. Psychiatry Neurol.* **2010**, 728052.
- [43] S. K. Badyal, J. Basran, N. Bhanji, J. H. Kim, A. P. Chavda, H. S. Jung, R. Craig, P. R. Elliott, A. F. Irvine, I. L. Barsukov, M. Kriajevska, C. R. Bagshaw, *J. Mol. Biol.* **2011**, *405*, 1004–1026.
- [44] J. A. Marsh, V. K. Singh, Z. Jia, J. D. Forman-Kay, *Protein Sci.* **2006**, *15*, 2795–2804.
- [45] Z. Hódi, A. L. Németh, L. Radnai, C. Hetényi, K. Schlett, A. Bodor, A. Perczel, L. Nyitray, *Biochemistry* **2006**, *45*, 12582–12595.
- [46] A. Bodor, L. Radnai, C. Hetényi, P. Rapali, A. Láng, K. E. Kövér, A. Perczel, W. Y. Wahlgren, G. Katona, L. Nyitray, *Biochemistry* **2014**, *53*, 7107–7122.
- [47] P. Kadeřávek, V. Zapletal, A. Rabatinová, L. Krásný, V. Sklenář, L. Židek, *J. Biomol. NMR* **2014**, *58*, 193–207.
- [48] T.-L. Hwang, P. C. M. van Zijl, S. Mori, *Biol. NMR* **1998**, *11*, 221–226.
- [49] G. Lipari, A. Szabó, *J. Am. Chem. Soc.* **1982**, *104*, 4546–4559.
- [50] G. Lipari, A. Szabó, *J. Am. Chem. Soc.* **1982**, *104*, 4559–4570.
- [51] G. M. Clore, P. C. Driscoll, P. T. Wingfield, A. M. Gronenborn, *Biochemistry* **1990**, *29*, 7387–7401.
- [52] G. M. Clore, A. Szabo, A. Bax, L. E. Kay, P. C. Driscoll, A. M. Gronenborn, *J. Am. Chem. Soc.* **1990**, *112*, 4989–4991.
- [53] R. Cole, J. P. Loria, *J. Biomol. NMR* **2003**, *26*, 203–213.
- [54] A. M. Mandel, M. Akke, A. G. Palmer III, *J. Mol. Biol.* **1995**, *246*, 144–163.
- [55] A. G. Palmer III, M. Rance, P. E. Wright, *J. Am. Chem. Soc.* **1991**, *113*, 4371–4380.
- [56] J. García de la Torre, M. L. Huertas, B. Carrasco, *J. Magn. Reson.* **2000**, *147*, 138–146.
- [57] D. M. Korzhnev, M. Billeter, A. S. Arseniev, V. Y. Orekhov, *Prog. Nucl. Magn. Reson. Spectrosc.* **2001**, *38*, 197–266.
- [58] N. A. Farrow, R. Muhandiram, A. U. Singer, S. M. Pascal, C. M. Kay, G. Gish, S. E. Shoelson, T. Pawson, J. D. Forman-Kay, L. E. Kay, *Biochemistry* **1994**, *33*, 5984–6003.
- [59] J. Cavanagh, W. J. Fairbrother, A. G. Palmer, M. Rance, N. J. Skelton, *Protein NMR Spectroscopy: Principles and Practice*, 2nd ed., Elsevier, San Diego, **2007**, pp. 21.
- [60] M. V. Berjanskii, D. S. Wishart, *J. Am. Chem. Soc.* **2005**, *127*, 14970–14971.
- [61] D. Yang, L. E. Kay, *J. Mol. Biol.* **1996**, *263*, 369–382.
- [62] R. Grünberg, M. Nilges, J. Leckner, *Structure* **2006**, *14*, 683–693.
- [63] R. B. Fenwick, H. van den Bedem, J. S. Fraser, P. E. Wright, *Proc. Natl. Acad. Sci. USA* **2014**, *111*, E445–E454.
- [64] D. D. Boehr, R. Nussinov, P. E. Wright, *Nat. Chem. Biol.* **2009**, *5*, 789–796.
- [65] P. Csermely, R. Palotai, R. Nussinov, *Trends Biochem. Sci.* **2010**, *35*, 539–546.
- [66] J. A. Marsh, S. A. Teichmann, J. D. Forman-Kay, *Curr. Opin. Struct. Biol.* **2012**, *22*, 643–650.
- [67] B. Kiss, L. Kalmár, L. Nyitray, G. Pál, *FEBS J.* **2016**, *283*, 2164–2180.
- [68] S. Mirzoeva, S. Weigand, T. J. Lukas, L. Shuvalova, W. F. Anderson, D. M. Watterson, *Biochemistry* **1999**, *38*, 3936–3947.
- [69] S. Tarabykina, D. J. Scott, P. Herzyk, T. J. Hill, J. R. H. Tame, M. Kriajevska, D. Lafitte, P. J. Derrick, G. G. Dodson, N. J. Maitland, E. M. Lukanidin, I. B. Bronstein, *J. Biol. Chem.* **2001**, *276*, 24212–24222.
- [70] A. C. Drohat, D. J. Weber, E. Nenortas, D. Beckett, *Protein Sci.* **1997**, *6*, 1577–1582.
- [71] A. L. Lee, S. A. Kinnear, A. J. Wand, *Nat. Struct. Biol.* **2000**, *7*, 72–77.
- [72] D. M. A. Smith, T. P. Straatsma, T. C. Squier, *Biophys. J.* **2012**, *103*, 1576–1584.
- [73] K. G. Hartman, L. E. McKnight, M. A. Liriano, D. J. Weber, *Future Med. Chem.* **2013**, *5*, 97–109.
- [74] R. L. J. Keller, *The Computer Aided Resonance Assignment Tutorial*, Cantina, Goldau, **2004**.
- [75] T. D. Goddard, D. G. Kneller, *SPARKY 3*, University of California, San Francisco, **2000**.

Manuscript received: May 12, 2016

Accepted article published: July 15, 2016

Final article published: August 24, 2016